Donor–acceptor–acceptor (D–A–A) type 1,8-naphthalimides as non-fullerene small molecule acceptors for bulk heterojunction solar cells†

Prabhat Gautam,[a] Rahul Sharma,[a] Rajneesh Misra,*[a] M. L. Keshtov,[b] S. A. Kuklin[b] and Ganesh D. Sharma*[c]

Donor–acceptor–acceptor (D–A–A) type 1,8-naphthalimide based small molecules **SM1** and **SM2** functionalized with tetracyanobutadiene (TCBD) and dicyanoquino-dimethane (DCNQ) modules, showing strong absorption in the visible and near-infrared (NIR) region are reported. TCBD and DCNQ linked **SM1** and **SM2** exhibit multi-redox waves. The electrochemical and optical HOMO–LUMO gaps show similar trends. These **SMs** exhibit a broad absorption profile which is complementary to the D–A copolymer **P** donor and also possess an appropriate lowest unoccupied molecular orbital (LUMO) to serve as an acceptor with **P** with a LUMO level of −3.33 eV. The organic solar cells based on **P:SM1** and **P:SM2** exhibit a PCE of 4.94% and 6.11%, respectively. The higher value of the PCE for the **SM2** based organic solar cells has been attributed to the broader absorption profile, more balanced charge transport and lower photon energy loss. The values of V_{oc} of the organic solar cells for the **SM1** acceptor (1.06 V and 1.02 V without and with solvent additive) are the highest values reported for devices based on non-fullerene acceptors to the best of our knowledge. The energy loss (E_{loss}) of 0.56 eV and 0.48 eV for **SM1** and **SM2** based devices, respectively is one of the smallest reported for BHJ organic solar cells.

Introduction

In most of the efficient organic solar cells, fullerene derivatives have been extensively used as acceptor materials along with conjugated polymers or small molecules as donors, because of their advantages of high electron mobility and affinity, isotropy of charge transport, and the ability to form favorable nanoscale networks with donor materials.[1] However, fullerene derivatives have certain drawbacks such as, poor photostability in air, poor solar energy harvesting, high production cost and difficulty in tuning the optical properties over a wide range of energy.[2]

Non-fullerene organic acceptors have been extensively used during the last couple of years due to their different structures, easier tunability of energy levels, good absorption and ease of synthesis.[3] High power conversion efficiencies (PCEs) in the range of 11–12% have been reported so far for OSCs based on non-fullerene organic acceptors.[4] In general, non-fullerene organic acceptors should have broad and strong absorptions in

the visible region of the solar spectrum, suitable HOMO/LUMO energy levels, good solubility is common organic solvents and high electron mobility. To achieve the above requirements, conjugated push–pull structures are used to construct non-fullerene acceptors, which could reduce the optical bandgap, extend absorption in the whole visible region of solar spectrum, and tune the energy levels. Moreover, to design a molecular system which exhibits effective intermolecular interactions is to have a large, planar and extended π-core which enhances π-stacking and reduces steric interactions. The supramolecular assembly of perylene diimides (PDIs) and naphthalenediimides (NDIs) and other amide based conjugated molecules have been incorporated in molecular systems which provides a potential strategy to tune their optical and electrochemical properties. NDIs are fluorescent redox-active planar materials that have a relatively high electron affinity (comparable to fullerene).[5] Bloking *et al.* have reported a di-phthalimide containing small molecule with benzothiadiazole as the core and used it as an acceptor along with P3HT as an electron donor for the fabrication of bulk heterojunction (BHJ) organic solar cells and achieved a PCE of 2.54%.[6] Naphthalimide (NI) based n-type small molecules with high electron mobility and low lying LUMO energy levels are promising acceptor materials for wide bandgap polymer based solar cells. Kwon *et al.* synthesized a dicyanodistyrylbenzene-naphthalimide (DCS-NI) type molecular acceptor and used it as a promising non-fullerene acceptor with good electron accepting properties and compatibility with

[a]*Department of Chemistry, Indian Institute of Technology Indore, Indore 453552, India. E-mail: rajneeshmisra@iiti.ac.in*

[b]*Institute of Organoelement Compounds of the Russian Academy of Sciences, Vavilova St., 28, 119991 Moscow, Russian Federation*

[c]*Department of Physics, LNM Institute of Information Technology, Jamdoli, Jaipur 302031, Rajasthan, India. E-mail: gdsharma273@gmail.com*

† Electronic supplementary information (ESI) available: Copies of ^{1}H, ^{13}C NMR and HRMS spectra of new compounds. The DFT calculation data of **SM1** and **SM2**. See DOI: 10.1039/c6sc04461a

both a polymer (P3HT)[7] and a small molecule donor (p-DTS(FBTTH₂)₂),[8] exhibiting a PCE of 2.71% and 5.44%, respectively. Chatterjee introduced a strong electron withdrawing group (naphtha[1,2-*c*:5,6-*c'*]bis[1,2,5]thizdiazole) in the di-naphthalimide system and successfully decreased the bandgap to 1.73 eV. The OSC devices exhibited a PCE of 2.81% by blending this with P3HT.[9] Bo *et al.* have developed a series of NI based non-fullerene acceptors with PCEs of 2–3% when blended with a wide band gap polymer.[10]

The electron deficient 1,8-naphthalimide (NI) unit exhibits high electron affinity and high charge carrier mobility, and acts as an acceptor unit.[11] However the D–A systems based on NIs have a wide energy gap.[12] The electronic and photonic properties of the D–A NIs can be tuned by substitution at the C-4 or C-5 position.[13] Recently cross conjugation has been utilized as a facile methodology to design low HOMO–LUMO gap molecular systems.[14,15] A variety of cross conjugated 1,1,4,4-tetracyanobutadienes (TCBD) and dicyanoquinodimethane (DCNQ) derivatives have been synthesized *via* the [2 + 2] cycloaddition–retroelectrocyclization reaction between donor substituted alkynes and tetracyanoethylene (TCNE) and tetracyanoquinodimethane (TCNQ).[16–18] The substitution of –CN in the molecular backbone can increase the electron affinity and promote the formation of a crystallite architecture by secondary interaction and/or local dipole alignments that favour efficient charge transport and also broaden the absorption profile towards a longer wavelength region, where the power density of the solar spectrum is higher.[19]

In this contribution, we wish to report triphenylamine-functionalized molecular systems of the type D–A₁–A₂. The triphenylamine substituted naphthalimide **3** was synthesized by the Pd-catalyzed Sonogashira cross-coupling reaction of compound **1** with 4-bromo-*N,N*-diphenylaniline **2**. The reaction of NI **3** with TCNE and TCNQ resulted in **SM1** and **SM2** with strong intramolecular charge transfer. The introduction of TCNQ in the small molecule, *i.e.* **SM2** showed a broader absorption profile extending up to 850 nm, attributed to the stronger electron withdrawing nature of TCNQ relative to TCNE. Both **SM1** and **SM2** possess relatively high lying LUMO energy levels than that of PC₇₁BM, which would produce a high open circuit voltage, when used as an acceptor along with the conjugated D–A copolymer **P** (the chemical structure is shown in Scheme 1). After the optimization of the active layer (weight ratio and concentration of solvent additive), the devices based on **P:SM1** and **P:SM2** showed PCEs of 4.94% and 6.11% with a high V_{oc} of 1.02 V and 0.92 V, respectively. Our results showed that these NI based small molecules can be potential acceptors for efficient organic solar cells using a copolymer and small molecule as donors.

Results and discussion

Synthesis of SM1 and SM2

The NI **1** was synthesized by the Pd-catalyzed Sonogashira coupling reaction of 4-bromo-1,8-naphthalimide with trimethylsilylacetylene followed by base catalyzed deprotection.[20,21] The Sonogashira cross-coupling reactions of compound **1**

with 4-bromotriphenylamine **2** resulted in compound **3** (Scheme 1).[21,22] The naphthalimide based small molecules **SM1** and **SM2** were synthesized by the [2 + 2] cycloaddition–retroelectrocyclization reaction of compound **3** with tetracyanoethylene (TCNE) and 7,7,8,8-tetracyanoquinodimethane (TCNQ). The [2 + 2] cycloaddition–retroelectrocyclization reaction of NI **3** with one equivalent of TCNE in dichloromethane (DCM) resulted in **SM1** in 65% yield (Scheme 1).[23] The reactions of 7,7,8,8-tetracyanoquinodimethane (TCNQ) with NI **3** was carried out under microwave irradiation due to its sluggish nature. The reaction of NI **3** with one equivalent of TCNQ in 1,2-dichloroethane (DCE) at 100 °C under microwave irradiation for 48 h resulted in **SM2** in 60% yield. **SM1** and **SM2** were purified by silica-gel column chromatography and well characterized by ¹H, ¹³C NMR, and HRMS techniques (details are summarized in ESI†).

Photophysical properties

The electronic absorption spectra of **SM1** and **SM2** were recorded in chloroform at room temperature (Fig. 1) and the data are listed in Table 1. These **SMs** exhibit two sets of absorption bands. The high energy absorption band between 330–414 nm corresponding to the π–π* transition was observed and the intramolecular charge transfer (ICT) transition was observed above 450 nm.[11a,12] The incorporation of 1,1,4,4-tetracyanobutadiene (TCBD) and dicyanoquinodimethane (DCNQ) acceptor units result in a strong ICT band in **SM1** and **SM2**. The small molecule **SM2** exhibits a substantial bathochromic shift of the onset absorption wavelength when compared to **SM1**, which can be attributed to the presence of the strong electron withdrawing DCNQ unit.[23] The absorption spectra of both **SM1** and **SM2** in a thin film show a redshift when compared to their absorption bands in solution due to the strong intermolecular interactions and effective solid state packing between the molecular backbones. The optical bandgaps estimated from the onsets of the absorption spectra in the thin films are 1.58 eV and 1.39 eV, for **SM1** and **SM2**, respectively. Since both small molecules have the same D and A₂, but different A₁ (TCBD and DCNQ for **SM1** and **SM2**, respectively), this difference may be attributed to the stronger withdrawing nature of DCNQ, relative to TCBD. The incorporation of the DCNQ acceptor unit results in a lower optical band gap for **SM2** as compared to **SM1**, which indicates that the optical band gap is a function of acceptor strength in these triphenylamine-substituted napthalimides.

To maximize the light harvesting efficiency of BHJs, integrating electron donors and electron acceptors with complementary light absorption is advantageous. Therefore we have used the D–A conjugated copolymer **P**, which has an absorption peak around 578 nm (as shown in Fig. 1), which is blue-shifted compared to the **SMs**. The absorption spectra of the **P** donor and **SM** acceptors complement each other.

Electrochemical properties

The electrochemical properties of triphenylamine-substituted napthalimides **SM1** and **SM2** were explored by cyclic voltammetric (CV) analysis in chloroform solution using tetrabutylammonium
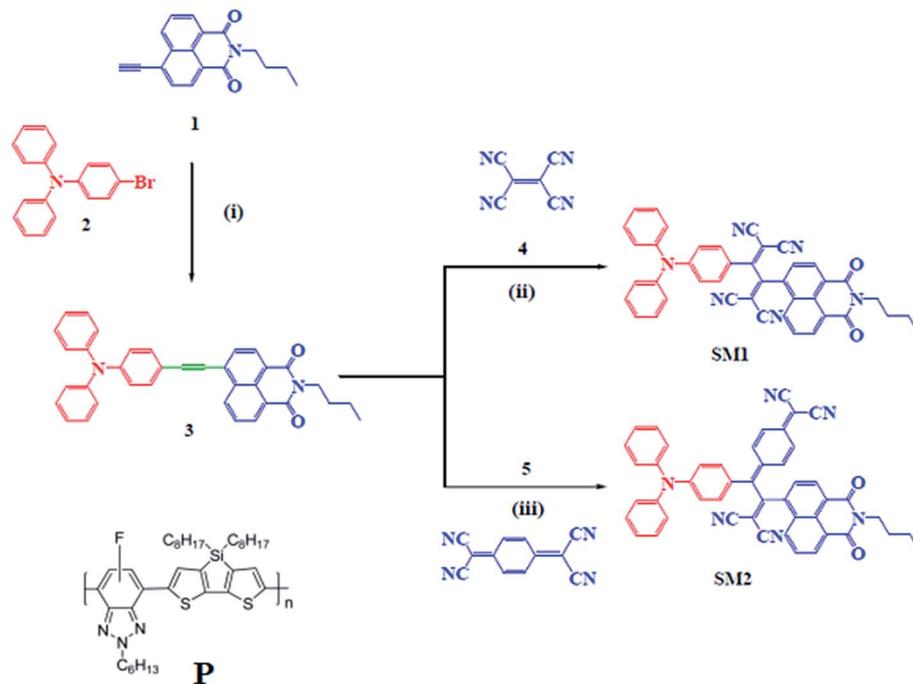
Scheme 1 Synthesis of triphenylamine-substituted 1,8-naphthalimides **SM1** and **SM2**. Reaction conditions: (i) $PdCl_2(PPh_3)_2$, CuI, THF : TEA (1 : 1), 70 °C, 15 h; (ii) CH_2Cl_2, 40 °C, 20 h. (iii) $C_2H_4Cl_2$, 100 °C, 48 h. The chemical structure of the D–A conjugated polymer is also shown.
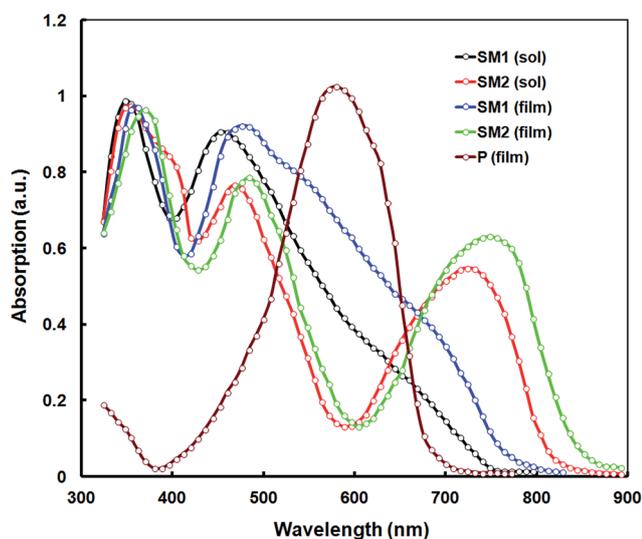
Fig. 1 Normalized absorption spectra of **SM1** and **SM2** in dilute chloroform solution and thin film cast from chloroform and the absorption spectra of **P** is also shown.

hexafluorophosphate (Bu_4NPF_6) as the supporting electrolyte. The electrochemical data are listed in Table 1 and the cyclic voltammograms of **SM1** and **SM2** are shown in Fig. 2.

SM1 and **SM2** exhibit multi-step redox waves corresponding to the reduction of naphthalimide, TCBD and DCNQ acceptor units, and the triphenylamine donor unit.[11a,12b] We have estimated the HOMO energy levels of **SM1** and **SM2** from $E_{HOMO} = -q(E_{oxid}^{onset} + 4.44)$ eV, where E_{oxid}^{onset} is the onset oxidation potential observed in cyclic voltammetry. The value of the HOMO energy

levels for **SM1** and **SM2** are −5.56 eV and −5.44 eV, respectively. The LUMO energy levels of **SM1** and **SM2** were estimated according to $E_{LUMO} = E_{HOMO} + E_g^{sol}$ and are −3.92 eV and −3.98 eV, respectively. The electrochemical studies show that the substitution of the DCNQ linkage in **SM2** results in a lower E_{elec} as compared to TCBD linked **SM1**. The HOMO/LUMO energy levels of the conjugated copolymer **P** used as an electron acceptor are −5.30/−3.33 eV, therefore, the LUMO offsets between **P** and the acceptors **SM1** and **SM2** are 0.61 eV and 0.53 eV, respectively and are greater than the threshold value of 0.3 eV, indicating that these small molecules can be employed as electron acceptors for the BHJ PSCs along with **P** as the donor. Compared to the LUMO energy level of $PC_{71}BM$ (−4.1 eV), these **SMs** possessed high lying LUMO levels. When **SM1** and **SM2** were used as acceptor materials, a decreased offset values between the LUMO level of **P** and **SMs** reduced the energy loss, resulting in a higher V_{oc} and PCE for the devices.[24]

Since the light absorption by the acceptors also contribute to the overall photocurrent generation of the devices, the hole transfer from the donor polymer **P** to acceptors needed to be considered. However, the HOMO offset is only 0.26 eV and 0.14 eV for **SM1** and **SM2**, respectively, which is smaller than the widely used empirical threshold value of 0.3 eV. Although these systems have a small HOMO offset, these system showed efficient hole transfer from the acceptors (**SM1** or **SM2**) to the conjugated polymer donor, which was confirmed by the IPCE values of the devices in the wavelength region beyond 650 nm where the light absorption by **P** is negligible,[25] indicating that both the conjugated polymer **P** and small molecules contribute equally to photocurrent generation in the devices. In the literature, it has been reported that a small HOMO off set of 0.1 eV

Table 1 Photophysical and electrochemical data of **SM1** and **SM2**

Compound	$\lambda_{abs}{}^a$ (nm)	ε (M^{-1} cm^{-1})	$E_{ox}{}^b$ (V)	$E_{red}{}^b$ (V)	$E_{elec}{}^c$ (eV)	$E_{op}{}^d$ (eV)
SM1	346	38 360	1.14	−0.32	1.44	1.64
	451	34 590		−0.76		
				−1.01		
SM2	353	34 098	0.98	−0.10	1.30	1.46
	467	26 994		−0.29		
	722	18 661		−1.10		

[a] Absorbance measured in chloroform at 1×10^{-5} M concentration; λ_{abs}: maximum absorption wavelength; ε: extinction coefficient. [b] E_{ox} and E_{red} are oxidation and reduction potentials. [c] E_{elec} is the electrochemical band gap estimated by using the onset oxidation and reduction potential. [d] E_{op} is the optical energy band gap estimated from the onset wavelength of the optical absorption in a dilute solution of chloroform (10^{-5}), using the formula $E_{op} = 1240/\lambda_{onset}$ where λ_{onset} is onset wavelength.
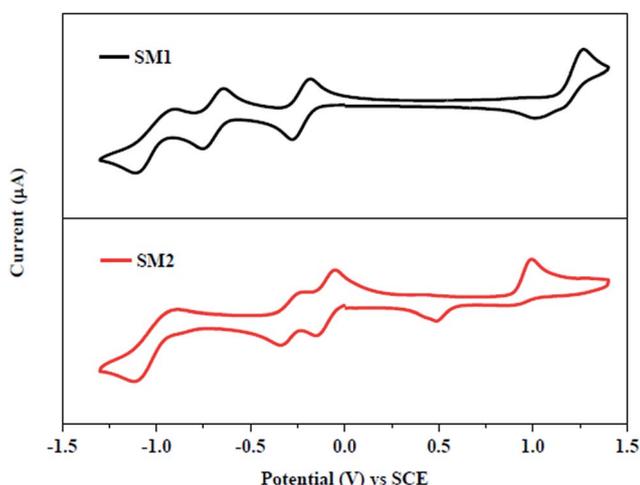
Fig. 2 Cyclic voltammogram of **SM1** and **SM2** at 0.01 M concentration in 0.1 M Bu_4NPF_6 in chloroform recorded at a scan rate of 100 mV s^{-1}.

could be sufficient in separating the charge carriers in non-fullerene PSCs.[26]

Theoretical calculations

In order to explore the electronic structure of **SM1** and **SM2**, density functional theory (DFT) calculations were performed at the B3LYP/6-31G** level.[27] The contours of the HOMO and LUMO of **SM1** and **SM2** are shown in Fig. 3, the HOMO is localized on the electron donating triphenylamine unit. The incorporation of the TCBD and DCNQ acceptor unit in **SM1** and **SM2** results in delocalization of the LUMO over the TCBD, DCNQ and 1,8-naphthalimide acceptor units. The substitution of the strongly electron withdrawing DCNQ acceptor unit in **SM2** results in a lower HOMO–LUMO gap and a red shift in the electronic absorption as compared to **SM1**. The values of the HOMO and LUMO energy levels are well in agreement with the estimated values from the cyclic voltammetry.

Photovoltaic properties

To demonstrate the potential applications of **SM1** and **SM2** as acceptors in polymer solar cells, we blended these with the previously reported D–A copolymer **P** as a donor and fabricated

BHJ PSCs with a device structure of ITO/PEDOT:PSS/**P**:**SM1** or **SM2**/PFN/Al.[28] The copolymer exhibited a D–A structure with dibromide 2-hexyl-4,7-dibromo-5-fluorobenzo-1,2,3-triazole and 4,4′-bis(2-ethylhexyl)-5,5′-bis(trimethyltin)-dithieno[3,2-*b*:2′,3′-*d*] silole acceptor and donor units respectively. The copolymer **P** exhibits a strong absorption band with an absorption maxima at 578 nm in the thin films, which is complementary to the absorption profiles of the **SMs** and suitable for the benefit of a higher light harvesting efficiency, when blended with these **SMs** as acceptors (the absorption spectra of the BHJ active layer cast from chloroform is shown in Fig. 4). In order to optimize the device performance, the effect of different D/A weight ratios and the concentration of the additive were investigated. The current–voltage characteristics of the optimized PSCs are shown in Fig. 5 (top) and corresponding data are summarized in Table 2. Without the use of an additive, the device based on **P** : **SM1** (1 : 1) and **P**:**SM2** showed overall PCEs of 2.34% (J_{sc} = 6.14 mA cm^{-2}, V_{oc} = 1.06 V and FF = 0.36) and 3.14% (J_{sc} = 8.02 mA cm^{-2}, V_{oc} = 0.98 V and FF = 0.40), respectively. After the addition of 3% DIO additive, the performance of the devices was
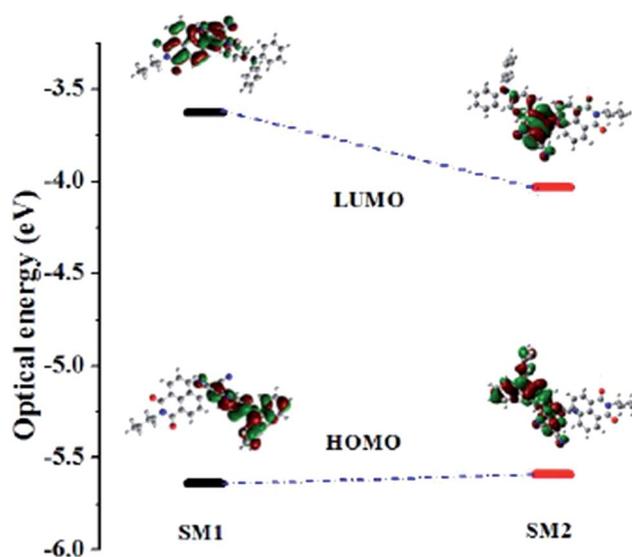
Fig. 3 Correlation diagram showing the HOMO and LUMO wave functions and energies of **SM1** and **SM2** as determined at the B3LYP/6-31G** level (iso value = 0.02).
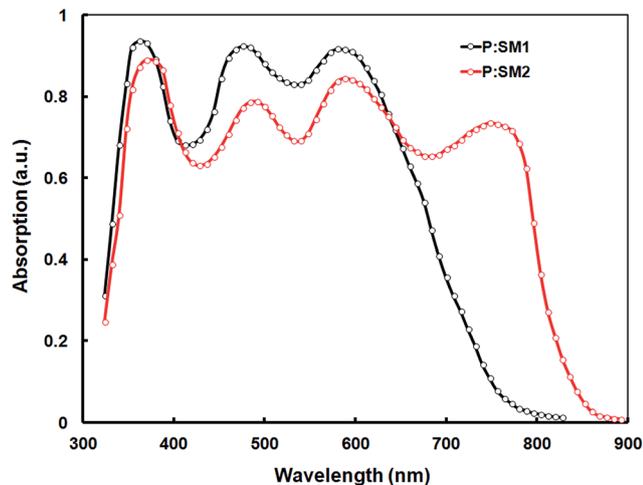
Fig. 4 Normalized absorption spectra of **P:SM1** and **P:SM2** in thin films cast from chloroform.
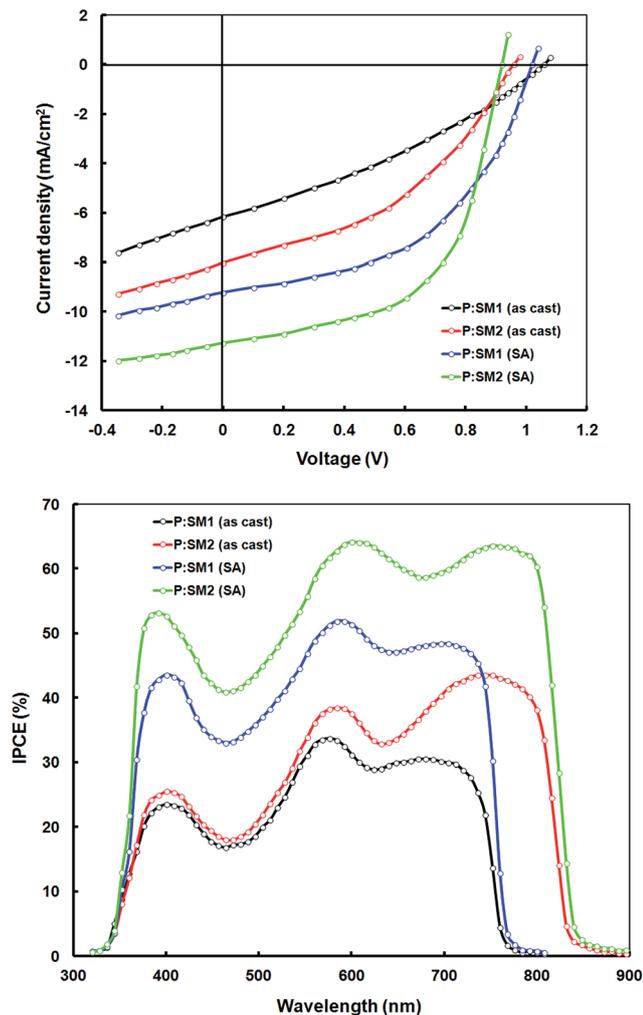
Fig. 5 Current−voltage (J−V) characteristics under illumination (Top) and IPCE spectra of the devices based on **P:SM1** and **P:SM2** (Bottom).

significantly improved to 4.94% ($J_{sc} = 9.15$ mA cm^{-2}, $V_{oc} = 1.02$ V and FF = 0.54) and 6.11% ($J_{sc} = 11.25$ mA cm^{-2}, $V_{oc} = 0.92$ V and FF = 0.59) for **SM1 :P** and **SM2:P** respectively.

The PCEs of **SM2** based devices is higher than that of their **SM1** counterparts, primarily in terms of the enhanced J_{sc} and FF, which might be attributed to the broader absorption profile of **SM2**, which can facilitate the harvesting of more solar photons, enhanced electron mobility, optimal active layer morphology or combination of these factors. In order to explain these issues, we have measured the optical absorption spectra of the BHJ active layers (*i.e.* optimized **P:SM1** and **P:SM2**) and these are shown in Fig. 4. It is noted that both the active layers showed absorption peaks corresponding to **P** and **SMs**, indicating that both the **P** donor and **SM** acceptors are contributing to exciton generation and thereby the J_{sc} of the devices. The absorption spectra of **P:SM1** and **P:SM2** is extended up to 770 nm and 850 nm, respectively, which can contribute to the enhanced J_{sc}.

We have measured the incident photon to current conversion efficiency (IPCE) response of the devices to verify the accuracy of the J_{sc} value obtained from the J–V characteristics and this is shown in Fig. 5 (bottom). The IPCE spectra of the devices closely resemble the absorption spectra of corresponding active layer (Fig. 4) demonstrating that both **P** and the SM acceptors contributed to photocurrent generation. Moreover, the IPCE values are significantly higher for the devices based on solvent additive processed active layers than the devices processed only from the chloroform solvent. The J_{sc} values estimated from the integration of the IPCE spectra are shown in Table 2, which are consistent with that obtained from the J–V characteristics of devices under illumination.

The V_{oc} of the device based on the **SM1** acceptor is higher than that of **SM2**, which is consistent with the reduced electron affinity (LUMO) of **SM1** as compared to **SM2**, since the V_{oc} of BHJ organic solar cells is directly related to the energy difference between the LUMO of the acceptor and the HOMO of the donor component employed in the active BHJ thin film. The value of V_{oc} which is about 1.06 and 1.02 V for the **SM1** acceptor is one of the highest values reported for devices based on non-fullerene acceptors.[29] Moreover, the energy loss (E_{loss}) of 0.56 eV and 0.47 eV ($E_{loss} = E_{opt}^{min} - qV_{oc}$, where E_{opt}^{min} is the smallest optical bandgap of either the donor or acceptor) for **SM1** and **SM2** based devices, respectively is one of the smallest reported for BHJ organic solar cells.[30] Recently, Liu *et al.* reported a PCE of 9.7% for a non-fullerene organic solar cell with low energy loss.[31]

We have also examined the charge carrier mobility (hole and electron) of the active layers, based on the space charge limited

Table 2 Photovoltaic parameters of the organic solar cells based on **P:SM1** and **P:SM2**

Active layer	J_{sc} (mA cm^{-2})	V_{oc} (V)	FF	PCE (%)
P:SM1 (as cast)	6.14	1.06	0.36	2.34 (2.23)[a]
P:SM2 (as cast)	8.02	0.98	0.40	3.14 (3.06)[a]
P:SM1 (SA)	9.15	1.02	0.54	4.94 (4.86)[a]
P:SM2 (SA)	11.26	0.92	0.59	6.11 (6.07)[a]

[a] Average of eight devices.

current model, in order to get information about the charge transportation in the devices. The hole mobility (μ_h) and electron mobility (μ_e) were measured by hole only devices with a structure of ITO/PEDOT:PSS/**P:SM1** or **SM2**/Au and electron only devices with a configuration of glass/Al/PEDOT:PSS/**P:SM1** or **SM2**/Al. After acquiring the J–V characteristics in the dark (Fig. 6a and b for hole only and electron only devices, respectively), these curves were fitted by Mott–Gurney equation: $J = 9\varepsilon_0\varepsilon_r\mu V^2/8L^3$. The μ_h/μ_e of the casted active layer **P:SM1** and **P:SM2** are $7.23 \times 10^{-5}/1.45 \times 10^{-6}$ cm^2 V^{-1} s^{-1} and $7.64 \times 10^{-5}/3.67 \times 10^{-6}$ cm^2 V^{-1} s^{-1}, respectively. The low value of the electron mobilities for both active layers induces the mismatch between the μ_h and μ_e and causes the unbalanced charge transport in the active layer and leads to a lower J_{sc} and FF for the devices based on the casted active layers.[32] After solvent additives, μ_h of **P:SM1** and **P:SM2** slightly increase up to 8.78×10^{-5} and 9.23×10^{-5} cm^2 V^{-1} s^{-1}, respectively, but μ_e for **P:SM1** and **P:SM2** increases significantly up to 3.45×10^{-5} and 5.78×10^{-5} cm^2 V^{-1} s^{-1}, respectively. The more pronounced increase in μ_e provides a more balanced charge transport in the active layer processed with solvent additives which leads to a higher J_{sc} and FF of the resulting OSCs.
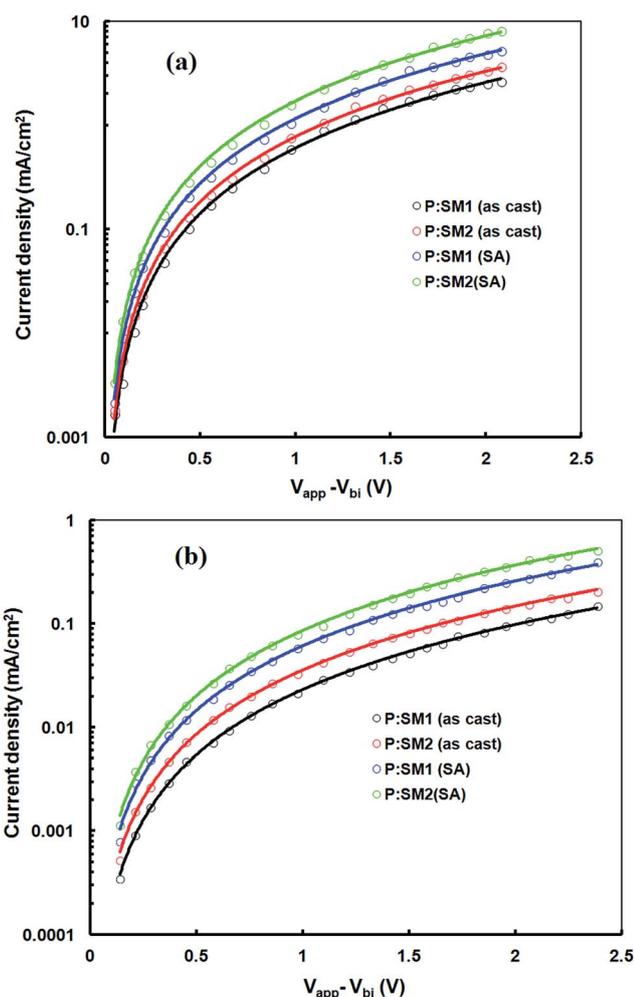
In order to investigate the exciton dissociation and photo-current generation in optimized devices based on **SM1** and **SM2** (only for DIO additive), the photocurrent density (J_{ph}) is plotted as a function of effective voltage (V_{eff}) for all the devices, as reported in the literature and shown in Fig. 7.[33] The J_{ph} is defined as $J_{ph} = J_L - J_D$, where J_L and J_D are the current densities under illumination and in the dark, respectively, V_{eff} is the given by $V_{eff} = V_0 - V_{appl}$, where V_0 is the voltage at which J_{ph} is zero and V_{appl} is the applied voltage. As shown in Fig. 7, J_{ph} increase linearly with V_{eff} in the low voltage region and reaches a plateau at high V_{eff}. Therefore, we assume that at full saturation, all the excitons generated after photon absorption in the active layer are dissociated into free charge carriers and are subsequently collected by the respective electrodes. This allows us to estimate the maximum exciton generation and dissociation rate G_{max} according to $J_{phsat} = qG_{max}L$, where q is the elementary charge and L is the thickness of the active layer. The values of G_{max} for **SM1** and **SM2** based devices are 8.0×10^{27} m^{-3} s^{-1} and 9.4×10^{27} m^{-3} s^{-1}, respectively. The trend observed for G_{max} for these devices is consistent with the enhancement of J_{sc} and IPCE spectra, indicating more exciton generation and dissociation in the **SM2** based device. In addition, a charge collection probability (P_c) ($P_c = J_{sc}/J_{phsat}$) of 0.87 was obtained for the device based on **SM2** and this is higher than that for the **SM1** based device (0.76). The decreased bimolecular recombination and increased exciton dissociation contributed to the high J_{sc} and FF of the device.

In order to get information about the difference in the morphologies of the active layers based on **P:SM1** and **P:SM2** the TEM images of thin films processed with the solvent additive are shown in Fig. 8. The blended film of **P:SM2** showed a much finer texture than **P:SM1** which was processed under similar conditions. This morphology is beneficial for exciton dissociation, charge transfer between the **SM2** acceptor to **P** (*vice versa*) and more effective charge transport in the **P:SM2** active layer which results in increased J_{sc} and FF. However, the TEM image

Fig. 6 Current–voltage characteristics in dark (a) hole only devices and (b) electron only devices.
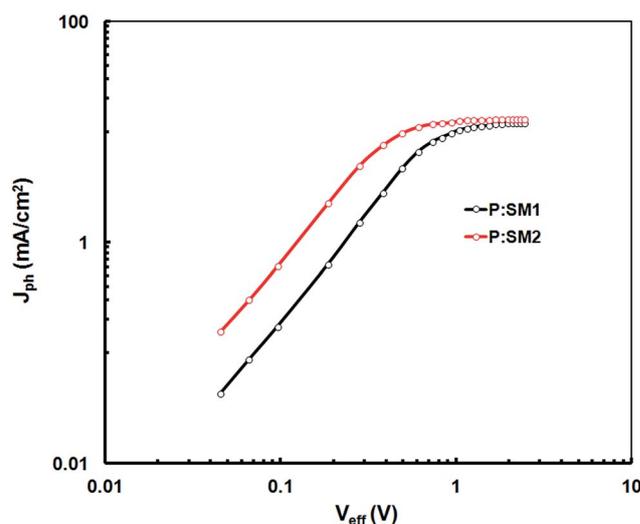
Fig. 7 Variation of J_{ph} with V_{eff} for the devices based on **P:SM1** and **P:SM2** processed with SA (DIO/CF).
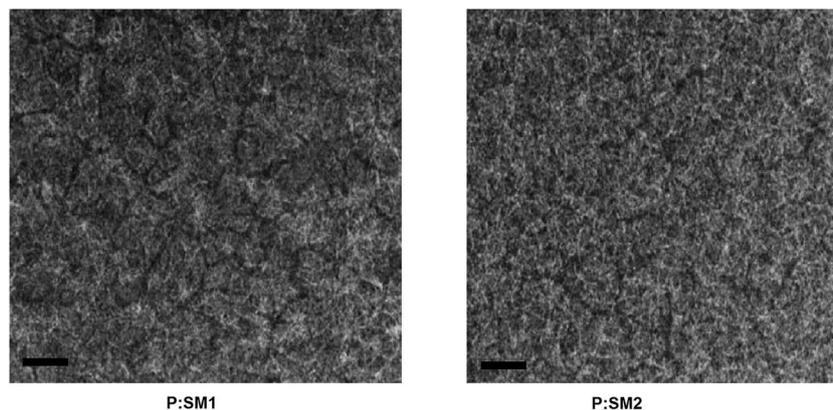
Fig. 8 TEM images of optimized **P:SM1** and **P:SM2** thin films processed with solvent additives. Scale bar is 200 nm.

of the **P:SM1** film showed a morphology with highly crystalline domains that hamper the exciton dissociation, resulting in relatively lower values of J_{sc} and FF.

Conclusion

In summary, donor–acceptor–acceptor (D–A–A) non-fullerene acceptors based on triphenylamine-substituted 1,8-naphthalimides derivatives **SM1** and **SM2** were designed and synthesized *via* [2 + 2] cycloaddition reaction of **3** with TCNE and TCNQ followed by subsequent ring-opening of the initially formed cyclobutene derivatives. The photophysical and electrochemical studies were performed to investigate the effect of acceptor strength modulation. The substitution of the acceptor DCNQ unit significantly lowers the HOMO–LUMO gap and results in a red shift of the absorption in the NIR region. The broad absorption, multi-step reduction waves and low HOMO–LUMO gap values make TCBD and DCNQ cross-conjugated NIs potential candidates for organic photovoltaics. The LUMO energy levels of these small molecules are about −3.94 and −3.98 eV and similar to that of $PC_{71}BM$, which is used as an acceptor along with conjugated D–A copolymer **P** as a donor. After the optimization of the donor to acceptor weight ratio and solvent additive concentration, the organic solar cells based on **P:SM1** and **P:SM2** exhibit PCEs of 4.94% and 6.11%, respectively. The results obtained in this study will be useful for the design and synthesis of non-fullerene acceptor materials with a low HOMO–LUMO gap and for BHJ organic solar cells.

Acknowledgements

References

1 (a) J. B. You, L. T. Dou, K. Yoshimura, T. Kato, K. Ohya, T. Moriarty, K. Emery, C. C. Chen, J. Gao, G. Li and Y. Yang, *Nat. Commun.*, 2013, **4**, 1446; (b) J. D. Chen, C. Cui, Y. Q. Li, L. Zhou, Q. D. Ou, C. Li, Y. Li and J. X. Tang, *Adv. Mater.*, 2015, **27**, 1035; (c) B. Kan, M. Li, Q. Zhang, F. Liu, X. Wan, Y. Wang, W. Ni, G. Long, X. Yang, H. Feng, Y. Zuo, M. Zhang, F. Huang, Y. Cao, T. P. Russell and Y. Chen, *J. Am. Chem. Soc.*, 2015, **137**, 3886.

2 (a) Y. Zhong, M. T. Trinh, R. Chen, W. Wang, P. P. Khlyabich, B. Kumar, Q. Xu, C. Y. Nam, M. Y. Sfeir, C. Black, M. L. Steigerwald, Y. L. Loo, S. Xiao, F. Ng, X. Y. Zhu and C. Nuckolls, *J. Am. Chem. Soc.*, 2014, **136**, 15215; (b) H. Li, Y. J. Hwang, B. A. E. Courtright, F. N. Eberle, S. Subramaniyan and S. A. Jenekhe, *Adv. Mater.*, 2015, **27**, 3266.

3 (a) A. F. Eftaiha, J. P. Sun, I. G. Hill and G. C. Welch, *J. Mater. Chem. A*, 2014, **2**, 1201; (b) C. Zhan, X. L. Zhang and J. Yao, *RSC Adv.*, 2015, **5**, 93002; (c) Y. Lin and X. Zhan, *Adv. Energy Mater.*, 2015, **5**, 1501063; (d) X. Guo, D. D. Tu and X. Liu, *J. Energy Chem.*, 2015, **24**, 675; (e) C. Zhan and J. Yao, *Chem. Mater.*, 2016, **28**, 1948.

4 (a) W. Zhao, Q. Qian, S. Zhang, S. Li, Q. Inganäs, F. Gao and J. Hou, *Adv. Mater.*, 2016, **28**, 4734; (b) S. Li, L. Ye, W. Zhao, S. Zhang, S. Mukherjee, H. Ade and J. Hou, *Adv. Mater.*, 2016, **28**, 9423.

5 N. Sakai, J. Mareda, E. Vauthey and S. Matile, *Chem. Commun.*, 2010, **46**, 4225–4237.

6 J. T. Bloking, X. Han, A. T. Higgs, J. P. Kastrop, L. Pandey, J. E. Norton, C. Risko, C. E. Chen, J. L. Brédas, M. D. McGehee and A. Sellinger, *Chem. Mater.*, 2011, **23**, 5484.

7 O. K. Kwon, J. H. Park, S. K. Park and S. Y. Park, *Adv. Energy Mater.*, 2015, **5**, 1400929.

8 O. K. Kwon, J. H. Park, D. W. Kim, S. K. Park and S. Y. Park, *Adv. Mater.*, 2015, **27**, 1951.

9 S. Chatterjee, Y. Ie, M. Karakawa and Y. Aso, *Adv. Funct. Mater.*, 2016, **26**, 1161.

10 (a) J. Zhang, X. Zhang, G. Li, H. Xiao, W. Li, S. Xie, C. Li and Z. Bo, *Chem. Commun.*, 2016, **52**, 469; (b) J. Zhang, X. Zhang,

H. Xiao, G. Li, Y. Liu, C. Li, H. Huang, X. Chen and Z. Bo, *ACS Appl. Mater. Interfaces*, 2016, **8**, 5475; (*c*) X. Zhang, J. Zhang, H. Lu, J. Wu, G. Li, C. Li, S. Li and Z. Bo, *J. Mater. Chem. C*, 2015, **3**, 6979.

11 (*a*) D. Gudeika, A. Michaleviciute, J. V. Grazulevicius, R. Lygaitis, S. Grigalevicius, V. Jankauskas, A. Miasojedovas, S. Jursenas and G. Sini, *J. Phys. Chem. C*, 2012, **116**, 14811; (*b*) F. Cacialli, R. H. Friend, C. M. Bouche, P. L. Barny, H. Facoetti, F. Soyer and P. J. Robin, *J. Appl. Phys.*, 1998, **83**, 2343; (*c*) E. Martin and R. A. Weigand, *Chem. Phys. Lett.*, 1998, **288**, 52; (*d*) C. Peebles, C. D. Wight and B. Iverson, *J. Mater. Chem. C*, 2015, **3**, 12156; (*e*) A. R. Mallia, P. S. Salini and M. Hariharan, *J. Am. Chem. Soc.*, 2015, **137**, 15604; (*f*) J. Zhang, H. Xiao, X. Zhang, Y. Wu, G. Li, C. Li, X. Chen, W. Ma and J. Bo, *J. Mater. Chem. C*, 2016, **4**, 5656; (*g*) A. Saini and K. R. J. Thomas, *RSC Adv.*, 2016, **6**, 71638.

12 D. Gudeika, J. V. Grazulevicius, D. Volyniuk, G. Juska, V. Jankauskas and G. Sini, *J. Phys. Chem. C*, 2015, **119**, 28335.

13 (*a*) J. L. Gu, E. Coronado, L. A. Martín, J. L. Montero, G. Fierro and J. M. García, *J. Phys. Chem. A*, 2007, **111**, 9724; (*b*) J. P. Malval, S. Suzuki, F. M. Savary, X. Allonas, J. P. Fouassier, S. Takahara and T. Yamaoka, *J. Phys. Chem. A*, 2008, **112**, 3879; (*c*) D. Kolosov, V. Adamovich, P. Djurovich, M. E. Thompson and C. Adachi, *J. Am. Chem. Soc.*, 2002, **124**, 9945; (*d*) O. K. Kwon, M. A. Uddin, J. H. Park, S. K. Park, T. L. Nguyen, H. Y. Woo and S. Y. Park, *Adv. Mater.*, 2016, **28**, 910; (*e*) J. Zhang, X. Zhang, G. Li, H. Xiao, W. Li, S. Xie, C. Li and Z. Bo, *Chem. Commun.*, 2016, **52**, 469.

14 W. C. W. Leu and C. S. Hartley, *Org. Lett.*, 2013, **15**, 3762.

15 (*a*) M. Gholami and R. R. Tykwinski, *Chem. Rev.*, 2006, **106**, 4997; (*b*) A. J. Zucchero, P. L. McGrier and U. H. F. Bunz, *Acc. Chem. Res.*, 2010, **43**, 397.

16 (*a*) S. Kato and F. Diederich, *Chem. Commun.*, 2010, **46**, 1994; (*b*) M. Kivala, T. Stanoeva, T. Michinobu, B. Frank, G. Gescheidt and F. Diederich, *Chem.–Eur. J.*, 2008, **14**, 7638; (*c*) T. Michinobu, I. Boudon, J. P. Gisselbrecht, P. Seiler, B. Frank, N. N. P. Moonen, M. Gross and F. Diederich, *Chem.–Eur. J.*, 2006, **12**, 1889.

17 T. Shoji, S. Ito, T. Okujimac and N. Moritad, *Org. Biomol. Chem.*, 2012, **10**, 8308.

18 S. Niu, G. Ulrich, P. Retailleau and R. Ziessel, *Org. Lett.*, 2011, **13**, 4996.

19 T. Zhou, T. Jia, B. King, F. Li, M. Fahlman and Y. Wang, *Adv. Energy Mater.*, 2011, **1**, 431.

20 S. Ast, T. Fischer, H. Müller, W. Mickler, M. Schwichtenberg, K. Rurack and H. J. Holdt, *Chem.–Eur. J.*, 2013, **19**, 2990.

21 H. Gao, Y. Li, L. Wang, C. Ji, Y. Wang, W. Tian, X. Yang and L. Yin, *Chem. Commun.*, 2014, **50**, 10251.

22 J. Li, F. Meng, H. Tian, J. Mi and W. Ji, *Chem. Lett.*, 2005, **34**, 922.

23 (*a*) R. Misra and P. Gautam, *Org. Biomol. Chem.*, 2014, **12**, 5448–5457; (*b*) P. Gautam, R. Misra, S. A. Siddiqui and G. D. Sharma, *ACS Appl. Mater. Interfaces*, 2015, **7**, 10283.

24 J. Zhang, X. Zhang, G. Li, H. Xiao, W. Li, S. Xie, C. Li and Z. Bo, *Chem. Commun.*, 2016, **52**, 469.

25 (*a*) H. Lin, S. Chen, Z. Li, J. Y. L. Lai, G. Yang, T. McAfcc, K. Jiang, Y. Li, Y. Liu, H. Hu, J. Zhao, W. Ma, H. Ade and H. Yan, *Adv. Mater.*, 2015, **27**, 7299; (*b*) Y. Li, L. Zhong, F. Wu, Y. Yuan, H. Bin, Z. Jiang, Z. Zhang, Z. Zhang, Y. Lim and L. Liao, *Energy Environ. Sci.*, 2016, **9**, 3429.

26 X. Gong, M. Tong, F. G. Brunetti, J. Seo, Y. Sun, D. Moses, F. Wudl and A. J. Heeger, *Adv. Mater.*, 2011, **23**, 2272.

27 M. J. Frisch; G. W. Trucks; H. B. Schlegel; G. E. Scuseria; M. A. Robb; J. R. Cheeseman; G. Scalmani; V. Barone; B. Mennucci; G. A. Petersson; H. Nakatsuji; M. Caricato; X. Li; H. P. Hratchian; A. F. Izmaylov; J. Bloino; G. Zheng; J. L. Sonnenberg; M. Hada; M. Ehara; K. Toyota; R. Fukuda; J. Hasegawa; M. Ishida; T. Nakajima; Y. Honda; O. Kitao; H. Nakai; T. Vreven; J. A. Montgomery Jr; J. E. Peralta; F. Ogliaro; M. Bearpark; J. J. Heyd; E. Brothers; K. N. Kudin; V. N. Staroverov; R. Kobayashi; J. Normand; K. Raghavachari; A. Rendell; J. C. Burant; S. S. Iyengar; J. Tomasi; M. Cossi; N. Rega; N. J. Millam; M. Klene; J. E. Knox; J. B. Cross; V. Bakken; C. Adamo; J. Jaramillo; R. Gomperts; R. E. Stratmann; O. Yazyev; A. J. Austin; R. Cammi; C. Pomelli; J. W. Ochterski; R. L. Martin; K. Morokuma; V. G. Zakrzewski; G. A. Voth; P. Salvador; J. J. Dannenberg; S. Dapprich; A. D. Daniels; O. Farkas; J. B. Foresman; J. V. Ortiz; J. Cioslowski and D. J. Fox, *Gaussian 09, revision A.02*, Gaussian, Inc., Wallingford, CT, 2009.

28 M. L. Keshtov, A. R. Khokhlov, S. A. Kuklin, I. E. Ostapov, A. Y. Nikolaev, I. O. Konstantinov, A. Sharma, E. N. Koukaras and G. D. Sharma, *Polym. Chem.*, 2016, **7**, 5849.

29 (*a*) T. Kim, J. H. Kim, T. E. Kang, C. Lee, H. Kang, M. Shin, C. Wang, B. Ma, U. Jeong, T. S. Kim and B. J. Kim, *Nat. Commun.*, 2015, **6**, 8547; (*b*) S. Li, H. Zhang, W. Zhao, L. Ye, H. Yao, B. Yang, S. Zhang and J. Hou, *Adv. Energy Mater.*, 2016, **6**, 1501991; (*c*) L. Gao, Z. G. Zhang, L. Xue, J. Min, J. Zhang, Z. Wei and Y. Li, *Adv. Mater.*, 2016, **28**, 1884.

30 (*a*) W. Li, K. H. Hendriks, A. Furlan, M. M. Wienk and R. A. J. Janssen, *J. Am. Chem. Soc.*, 2015, **137**, 2231; (*b*) K. Kawashima, Y. Tamai, H. Ohkita, I. Osaka and K. Takimiya, High-efficiency polymer solar cells with small photon energy loss, *Nat. Commun.*, 2015, **6**, 10085.

31 J. Liu, S. Chen, D. Qian, B. Gautam, G. Yang, J. Zhao, J. Bergqvist, F. Zhang, W. Ma, H. Ade, O. Inganäs, K. Gundogdu, F. Gao and H. Yan, *Nat. Energy*, 2016, **1**, 16089.

32 D. Gupta, S. Mukhopadhyay and K. Narayan, *Sol. Energy Mater. Sol. Cells*, 2010, **94**, 1309.

33 (*a*) C. M. Proctor, C. Kim, D. Neher and T. Q. Nguyen, *Adv. Funct. Mater.*, 2013, **23**, 3584; (*b*) P. W. M. Blom, V. D. Mihailetchi, L. J. A. Koster and D. E. Markov, *Adv. Mater.*, 2007, **19**, 1551; (*c*) V. D. Mihailetchi, H. X. Xie, B. de Boer, L. J. A. Koster and P. W. M. Blom, *Adv. Funct. Mater.*, 2006, **16**, 699.